Photolysis of CH3CHO at 248 nm: Evidence of triple fragmentation from primary quantum yield of CH3 and HCO radicals and H atoms

Pranay Morajkar, Adriana Bossolasco, Coralie Schoemaecker, and Christa Fittschen

Citation: The Journal of Chemical Physics **140**, 214308 (2014); doi: 10.1063/1.4878668
View online: http://dx.doi.org/10.1063/1.4878668
View Table of Contents: http://scitation.aip.org/content/aip/journal/jcp/140/21?ver=pdfcov
Published by the AIP Publishing

Photolysis of CH_3CHO at 248 nm: Evidence of triple fragmentation from primary quantum yield of CH_3 and HCO radicals and H atoms

Pranay Morajkar,[1] Adriana Bossolasco,[1,2] Coralie Schoemaecker,[1] and Christa Fittschen[1,a)]

[1]*Université Lille Nord de France, PhysicoChimie des Processus de Combustion et de l'Atmosphère – PC2A, UMR 8522, F-59650 Villeneuve d'Ascq, France*

[2]*INFIQC (CONICET), Departamento de Fisicoquímica, Facultad de Ciencias Químicas, Universidad Nacional de Córdoba, Córdoba, Argentina*

(Received 9 April 2014; accepted 7 May 2014; published online 3 June 2014)

Radical quantum yields have been measured following the 248 nm photolysis of acetaldehyde, CH_3CHO. HCO radical and H atom yields have been quantified by time resolved continuous wave Cavity Ring Down Spectroscopy in the near infrared following their conversion to HO_2 radicals by reaction with O_2. The CH_3 radical yield has been determined using the same technique following their conversion into CH_3O_2. Absolute yields have been deduced for HCO radicals and H atoms through fitting of time resolved HO_2 profiles, obtained under various O_2 concentrations, to a complex model, while the CH_3 yield has been determined relative to the CH_3 yield from 248 nm photolysis of CH_3I. Time resolved HO_2 profiles under very low O_2 concentrations suggest that another unknown HO_2 forming reaction path exists in this reaction system besides the conversion of HCO radicals and H atoms by reaction with O_2. HO_2 profiles can be well reproduced under a large range of experimental conditions with the following quantum yields: $CH_3CHO + h\nu_{248nm} \rightarrow CH_3CHO^*$, $CH_3CHO^* \rightarrow CH_3 + HCO \quad \phi_{1a} = 0.125 \pm 0.03$, $CH_3CHO^* \rightarrow CH_3 + H + CO \quad \phi_{1e} = 0.205 \pm 0.04$, $CH_3CHO^* \xrightarrow{O_2} CH_3CO + HO_2 \quad \phi_{1f} = 0.07 \pm 0.01$. The CH_3O_2 quantum yield has been determined in separate experiments as $\phi_{CH_3} = 0.33 \pm 0.03$ and is in excellent agreement with the CH_3 yields derived from the HO_2 measurements considering that the triple fragmentation (R1e) is an important reaction path in the 248 nm photolysis of CH_3CHO. From arithmetic considerations taking into account the HO_2 and CH_3 measurements we deduce a remaining quantum yield for the molecular pathway: $CH_3CHO^* \rightarrow CH_4 + CO \quad \phi_{1b} = 0.6$. All experiments can be consistently explained with absence of the formerly considered pathway: $CH_3CHO^* \rightarrow CH_3CO + H \quad \phi_{1c} = 0$.
 [http://dx.doi.org/10.1063/1.4878668]

I. INTRODUCTION

Acetaldehyde, CH_3CHO, is one of the important carbonyl compounds present in the atmosphere because its photodecomposition by sunlight generates free radicals, which further influence the photochemistry of the troposphere. Acetaldehyde is emitted to the atmosphere both through direct anthropogenic and biogenic emission, but is also generated during the photochemical oxidation of volatile organic compounds (VOC) such as alkanes and alkenes.[1] Concentrations of up to 100 ppt are even found at altitudes of 12 km. In a recent study,[2] average annual concentrations of CH_3CHO of 430 ppt were found in the tropic, remote marine boundary layer between 2006 and 2011, but current atmospheric models underestimate this concentration by up to a factor of 10, rising to 40 during the summer. This shows that the sources and sinks of acetaldehyde are still not well understood and it is important to further investigate the degradation mechanism of acetaldehyde. Photolysis is one of the possible degradation paths for CH_3CHO, and its photochemistry has been studied many times: the most detailed study using the analysis of stable end products has been carried out by Moortgat *et al.*,[3] who also developed a parameterization of quantum yields as a function of wavelength (250–330 nm) and pressure (100–870 Torr N_2).[4] Their end product analysis can be consistently interpreted with three different primary photolysis pathways:

$$CH_3CHO^* \rightarrow CH_3 + HCO, \qquad \text{(R1a)}$$

$$CH_3CHO^* \rightarrow CH_4 + CO, \qquad \text{(R1b)}$$

$$CH_3CHO^* \rightarrow CH_3CO + H. \qquad \text{(R1c)}$$

The wavelength dependant photochemistry of CH_3CHO has also recently attracted increased interest as it has become another model molecule for testing the concept of "roaming" mechanism, a new mechanism that has first been described for the photo-dissociation of CH_2O.[5] Houston and Kable[6] have analyzed the detailed state distribution of the nascent CO produced following 308 nm photolysis of CH_3CHO. They deduced that up to 15% of the CO originates from a mechanism other than the conventional transition state mechanism (R1b) and attributed it to the roaming pathway:

$$CH_3CHO^* \rightarrow (CH_3 + HCO) \xrightarrow{roaming} CH_4 + CO. \qquad \text{(R1d)}$$

a)Author to whom correspondence should be addressed. Electronic mail: christa.fittschen@univ-lille1.fr. Tel.: ++ 33 3 20 33 72 66. Fax: ++ 33 3 20 43 69 77.

The same group has since then undertaken other experiments and theoretical calculations,[7,8] confirming the importance of the roaming mechanism (R1d) in the photolysis of CH_3CHO at wavelengths above around 300 nm. Rubio-Lago *et al.* photolysed CH_3CHO at 248 nm and concluded from slice imaging detection[9] as well as later from a combination of velocity-map imaging and rotational resonance enhanced multiphoton ionization[10] of the product CO, that roaming is even more important at this shorter wavelength. From a lack of any CH_3 signal in both studies they conclude furthermore, that the roaming channel (R1d) competes very efficiently with the radical channel (R1a). A detailed review on the roaming mechanism in CH_3CHO photolysis can be found in Bowman and Shepler.[11] Recently, de Wit *et al.*[12] suggested another possible pathway following CH_3CHO photolysis, the triple fragmentation:

$$CH_3CHO^* \rightarrow CH_3 + H + CO, \qquad \text{(R1e)}$$

and deduced from theoretical considerations that such triple fragmentation would lead to cold translational and rotational reaction products, precisely the characteristics of the donating product in a roaming mechanism. From a thermodynamic point of view, triple fragmentation is open for CH_3CHO for wavelengths shorter than 294 nm. By only observing the CO fragment it would therefore be thinkable to attribute the cold CO from channel (R1e) to the roaming channel (R1d). Han *et al.*[13] recently presented quasiclassical trajectory calculations of the dissociation dynamics of CH_3CHO at high energies. They obtained branching ratios of 45.4%, 14.6%, 19.5%, and 9.9% for channels (R1a), (R1e), (R1b), and (R1c), respectively. An overall yield of 60% for CH_3 radicals has thus been predicted, in total contradiction with absence of any CH_3 signal in the experiments of Rubio-Lago *et al.*[9,10] In a very recent work, Hung *et al.*[14] applied time-resolved FTIR emission spectroscopy to investigate the roaming and triple fragmentation pathways following the 248 nm photolysis of CH_3CHO. From time-resolved measurements of the HCO fragment as well as the rotational distribution of CO they conclude to have the first experimental evidence of triple fragmentation following the 248 nm photolysis of CH_3CHO.

Considering the different results from experimental and theoretical works, new experiments aiming to observe the different possible photolysis products is needed. In the present work, we present the application of time resolved continuous wave Cavity Ring Down Spectroscopy (cw-CRDS) for the quantification of radical yields following the 248 nm photolysis of CH_3CHO. The yields of HCO radicals and H atoms, products of different reaction paths, are determined following their transformation into HO_2 radicals. The CH_3 radical yield is determined following its reaction with O_2 and conversion to CH_3O_2. Combination of CH_3, HCO and H yields can unravel the presence of triple fragmentation through unequal yields of CH_3 and HCO radicals.

II. EXPERIMENTAL TECHNIQUE

Experiments have been performed by laser photolysis coupled to a detection of HO_2 and CH_3O_2 radicals by cw-CRDS in the near infrared. The experimental set-up has already been described in previous papers[15–17] and only a brief description will be given here. Pulsed photolysis of acetaldehyde at 248 nm was carried out by an excimer laser (Lambda Physik LPX 202i). OH radicals were detected in some experiments to control acetaldehyde concentration or to cross check the photolysis energy (see further down) by high repetition rate LIF (10 kHz) using a frequency doubled YAG (Spectra Physics) pumped dye laser (SIRAH), operating at 10 kHz repetition rate with a maximum output power of 30 mW.[18] The absorption path for the detection of HO_2 or CH_3O_2 radicals by cw-CRDS is installed in a small angle (4°) with respect to the excimer laser beam, leading to an overlap of 28.7 cm between both laser beams. HO_2 concentration time profiles have been measured at total pressures of 10, 50, and 90 Torr He with O_2 between 0.05 and 10 Torr added to the mixture, CH_3O_2 profiles were measured at a total pressure of 50 and 100 Torr helium containing up to 100 Torr O_2. HO_2 concentration–time profiles were measured at the peak of the most intense absorption line in the $2\nu_1$ band[19] at 6638.205 cm^{-1}, CH_3O_2 profiles were recorded at one of the maxima in the ν_{12}-transition[20] at 7489.16 cm^{-1}. Time-resolved ring-down times, τ, have been converted into absorption coefficients, α, and subsequently into absolute concentrations by the following equation:

$$\alpha_t = \sigma \times [RO_2]_t = \frac{R_L}{c}\left(\frac{1}{\tau_t} - \frac{1}{\tau_0}\right), \qquad (1)$$

with R_L being the ratio between the cavity length L, i.e., the distance between the two cavity mirrors, to the length L_A over which the absorber is present (in our case the overlap of photolysis beam and absorption path), c is the speed of light, τ_0 and τ_t being the ring-down times before the photolysis pulse and at a delay t after the photolysis pulse, respectively. The absorption cross sections, σ, necessary in (1) to convert α into absolute concentrations, have been found pressure independent for the CH_3O_2 radical by Farago *et al.*[20] and a unique value of $\sigma_{CH_3O_2} = 3.4 \times 10^{-20}$ cm^2 has been used throughout the work. The helium pressure broadening of the HO_2 absorption line at 6638.205 cm^{-1} has been determined in the frame of this work and more details on the absorption cross sections employed to calculate absolute HO_2 concentrations can be found further down. Typical ring-down times in the empty cell, i.e., before the photolysis pulse, were around 50 μs for the HO_2 measurements, leading to ring-down times of around 35 μs for the highest HO_2 concentrations. Mirrors with lower reflectivity were used for the CH_3O_2 measurements and typical ring-down times of the empty cavity of only 16 μs were obtained, leading to ring-down times of around 14 μs for the highest CH_3O_2 concentrations.

The photolysis laser frequency was 0.3 Hz allowing refreshing the gas mixture between two laser pulses. The photolysis energy was measured at the exit of the photolysis cell using a power meter (Newport 841-PE), 10% were added to the measured value in order to take into account the loss through the exit window (determined in separate experiments). However, uncertainties of power meters are rather high, therefore photolysis energies were also cross-checked by measuring well-known systems. In the case of HO_2 radicals, both OH and HO_2 radical profiles were measured simultaneously following the photolysis of H_2O_2. From the

exponential decay of the relative OH profile (obtained by LIF), the initial H_2O_2 concentration can be retrieved using the known rate constant between OH radicals and H_2O_2 molecules, while fitting of the absolute HO_2 concentration time-profile (obtained by cw-CRDS) allows retrieving the initial, absolute OH-concentration. Admitting that the 248 nm photolysis of H_2O_2 leads to the formation of two OH-radicals,[21,22] the ratio between OH and H_2O_2 concentration in turn depends only on the well-known absorption cross section of H_2O_2 at 248 nm (9.06×10^{-20} cm^2)[23] as well as the photolysis energy (for more details see Jain *et al.*[24]) and hence allows retrieving the photolysis energy. On the other hand, the absolute HO_2 concentration, which is the basis for the ratio OH/H_2O_2, is extracted from equation (1) and depends thus on the correct R_L and σ: any systematic error in these values will be directly reflected in a proportional error in the retrieved photolysis energy. The photolysis energy obtained this way was in very good agreement (better than 10%) with the photolysis energy obtained from the corrected power meter readings. In the case of the CH_3O_2 radical measurements, the yield has not only been measured through determining absolute concentrations and photolysis energies, but has first and foremost been measured in back-to-back experiments relative to the CH_3O_2 yield following CH_3I photolysis. Also in these experiments, a comparison of the calculated photolysis energy from absolute CH_3O_2 measurement following the CH_3I photolysis with power meter measurements showed an excellent agreement, giving confidence to the power meter readings.

A. Reactants and concentration measurements

CH_3CHO (Sigma Aldrich, ≥99.5%) was prepared as a diluted gas mixture in a darkened glass bulb at concentrations of up to 2%. CH_3CHO is known to easily polymerize, therefore the CH_3CHO concentration within the balloon, deduced from pressure measurements, was occasionally verified by measuring OH-decays under pseudo-first order conditions. For these experiments, H_2O_2 has been co-photolyzed with CH_3CHO and the exponential OH-decay has been followed by LIF: using the well-known rate constant of the reaction between OH and CH_3CHO allows calculating the CH_3CHO concentration, such as detailed by Morajkar *et al.*[25] Helium (Praxair 6.0) and O_2 (Praxair 4.5) were used without further purification and have been added through calibrated flow meters. The lowest O_2 concentrations resulted from a small leak, carefully quantified before each experiment from a measurement of $\Delta p/\Delta t$ in a known volume, obtained by comparison with a known flow from calibrated flow meters.

III. RESULTS AND DISCUSSION

The results are presented in three sections: determination of the CH_3-radical quantum yield by quantifying the formation of CH_3O_2 radicals following the 248 nm photolysis of CH_3CHO in the presence of large excess O_2 in Sec. III A; determination of the helium pressure broadening of the HO_2 absorption line at 6638.205 cm^{-1}, necessary for retrieving absolute HO_2 concentrations at different pressures in Sec. III B, and determination of the H atom and HCO radical quantum yield through time resolved measurements of HO_2 radicals following the CH_3CHO photolysis in the presence of variable O_2 concentrations and at different pressures in Sec. III C.

A. CH_3 radical quantum yield from time resolved CH_3O_2 profiles

The CH_3 radical is the primary dissociation product of reaction channel (R1a) but is also formed in the recently postulated triple fragmentation pathway (R1e).[12] Determining the CH_3 radical yield and comparing it to the yield of HCO radicals is therefore interesting, as it allows estimating the importance of the triple fragmentation under our conditions: in absence of any triple fragmentation, the HCO and the CH_3 yields should be identical, while triple fragmentation at a non-negligible yield should result in a higher CH_3 radical yield compared to the HCO radical yield. An important yield of acetyl radicals, i.e., reaction (R1c), would on the other hand lead to an H-atom yield without the equivalent CH_3 yield.

We have detected CH_3 radicals following the 248 nm photolysis of CH_3CHO after conversion to CH_3O_2 radicals in the presence of excess O_2.

$$CH_3 + O_2(+M) \rightarrow CH_3O_2(+M). \qquad \text{(R2)}$$

Reaction (R2) converts CH_3 radicals under our O_2 concentrations into CH_3O_2 radicals within less than 10 μs, rendering radical-radical reactions such as (R6), (R9), (R10), or (R11) (see Table I) negligible at the overall low radicals concentrations. CH_3O_2 radicals have been detected by cw-CRDS in the near infrared at the ν_{12} transition at 7489.16 cm^{-1}. In a recent work, we have measured the absorption spectrum of CH_3O_2 radicals in this wavelength range[20] and absolute absorption cross sections a factor of 2–3 times higher than earlier determinations[26,27] have been obtained. In order to cross-check CH_3 yields, determined by calculating absolute CH_3O_2 concentrations using this absorption cross section together with the photolysis energy, we have carried out relative measurement: the CH_3O_2 concentration following the 248 nm photolysis of CH_3CHO was determined relative to the CH_3O_2 concentration following the 248 nm photolysis of CH_3I, always in the presence of excess O_2. For this purpose, diluted CH_3I and CH_3CHO mixtures in helium have been prepared in darkened glass bulbs, with the concentrations calculated from pressure measurements. As CH_3CHO is known to polymerize, its concentration has been cross-checked occasionally by measuring OH-decays, as described earlier. Back-to-back experiments have been carried out by photolysing alternately mixtures containing a known concentration of CH_3I or CH_3CHO, using the same photolysis energy. A typical example is presented Figure 1.

Under the assumption that all CH_3 radicals are converted to CH_3O_2, i.e., O_2 concentrations high enough to make reaction (R7) (see Table I) fast compared to secondary reactions, the absorption coefficient α, extrapolated to zero delay after the photolysis pulse, can be expressed for both species as

$$\alpha_{CH_3I,t=0} = [CH_3O_2] \times \sigma_{CH_3O_2}$$
$$= [CH_3I] \times \sigma_{CH_3I} \times F_{248nm} \times \phi_{CH_3I} \times \sigma_{CH_3O_2},$$

TABLE I. Complete reaction mechanism used to fit the HO_2 concentration time profiles.

Reaction		No.	k (cm^3 s^{-1})	Reference
$CH_3CHO + h\nu_{248\ nm}$	$\rightarrow CH_3 + HCO$	R1a	$\phi = 0.125$	
	$\rightarrow CH_3 + H + CO$	R1e	$\phi = 0.205$	This work
	$+ O_2 \rightarrow CH_3CO + HO_2$	R1f	$\phi = 0.07$	
	$\rightarrow CH_4 + CO$	R1b	$\phi = 0.6$	
$CH_3 + O_2$ (+M)	$\rightarrow CH_3O_2$ (+M)	R2	1.4×10^{-13}[a]	51, 52
$HCO + O_2$	$\rightarrow CO + HO_2$	R3	5.2×10^{-12}	28
$H + O_2$ (+M)	$\rightarrow HO_2$ (+M)	R4	3×10^{-14}[a]	44
$H + CH_3CHO$	$\rightarrow H_2 + CH_3CO$	R5	1.1×10^{-13}	46
$CH_3 + HCO$	$\rightarrow CH_4 + CO$	R6	2×10^{-10}	49
$H + HCO$	$\rightarrow H_2 + CO$	R7	1.5×10^{-10}	50
$H + HO_2$	$\rightarrow 2\ OH$	R8	8×10^{-11}	23
$2\ CH_3$	$\rightarrow C_2H_6$	R9	6×10^{-11}	53
$CH_3 + CH_3O_2$	$\rightarrow 2\ CH_3O$	R10	4.5×10^{-11}	49
$CH_3 + HO_2$	$\rightarrow CH_3O + OH$	R11	3.7×10^{-11}	54
$CH_3CHO + HO_2$	$\rightarrow CH_3CH(OH)O_2$	R12	1.5×10^{-14}	55
$CH_3CH(OH)O_2$	$\rightarrow CH_3CHO + HO_2$	R13	$900\ s^{-1}$	55
$CH_3O + O_2$	$\rightarrow CH_2O + HO_2$	R14	1.92×10^{-15}	28
$CH_3CO + O_2$	$\rightarrow OH + CH_2C(O)O$	R15a	1.05×10^{-12}[a]	56
	$\rightarrow CH_3C(O)O_2$	R15b	1.74×10^{-12}	
$CH_3O + CH_3CHO$	$\rightarrow CH_3CO + CH_3OH$	R16	7×10^{-14}	57
$2\ HO_2$	$\rightarrow H_2O_2 + O_2$	R17	1.7×10^{-12}	23
$2\ CH_3O_2$	$\rightarrow 2\ CH_3O + O_2$	R18a	1.3×10^{-13}	28
	$\rightarrow$ Products	R18b	2.2×10^{-13}	
$CH_3O_2 + HO_2$	$\rightarrow$ products	R19	5.2×10^{-12}	28
$CH_3C(O)O_2 + HO_2$	$\rightarrow CH_3 + OH$ [b]	R20a	6.16×10^{-12}	28[c]
	$\rightarrow$ products	R20b	7.57×10^{-12}	
$2\ CH_3C(O)O_2$	$\rightarrow 2\ CH_3$ [b]		1.6×10^{-11}	28
$CH_3C(O)O_2 + CH_3O_2$	$\rightarrow CH_3O + CH_3$ [b]		9.9×10^{-12}	28
	$\rightarrow$ products		1.1×10^{-12}	
$OH + CH_3CHO$	$\rightarrow H_2O + CH_3CO$		1.5×10^{-11}	28
$OH + CH_3O_2$	$\rightarrow$ products		2.8×10^{-10}	30
$CH_3CH(OH)O_2 + HO_2$	$\rightarrow$ products		1.2×10^{-11}	3
$CH_3CH(OH)O_2 + CH_3C(O)O_2$	$\rightarrow CH_3 + HO_2$ [b]		1×10^{-11}	3
$CH_3CH(OH)O_2 + CH_3O_2$	$\rightarrow HO_2 + CH_3O$ [b]		1.8×10^{-12}	3
	$\rightarrow$ products		1.2×10^{-12}	
$2\ CH_3CH(OH)O_2$	$\rightarrow 2\ HO_2$ [b]		5.4×10^{-12}	3
	$\rightarrow$ products		6×10^{-13}	
$CH_3CH(OH)O_2$	$\rightarrow$ diffusion		$5\ s^{-1}$	
HO_2	$\rightarrow$ diffusion		$7\ s^{-1}$	

[a]Rate constant at 50 Torr, values for 10 and 90 Torr have been adapted according to corresponding references.
[b]Reaction is not stoichiometric, only radical products influencing the HO_2 profiles are listed.
[c]A recent work of Groß *et al.*[58] suggests higher values, used for the dashed lines in Figure 6 (see text).

$$\alpha_{CH_3CHO,t=0} = [CH_3O_2] \times \sigma_{CH_3O_2} = [CH_3CHO] \times \sigma_{CH_3CHO} \times F_{248nm} \times \phi_{CH_3CHO} \times \sigma_{CH_3O_2},$$

with $\sigma_{CH_3O_2}$ the absorption cross section of CH_3O_2 radicals at 7489.16 cm^{-1}, σ_{CH_3I} and σ_{CH_3CHO} the absorption cross sections of CH_3I (8.07×10^{-19} cm^2)[28] and CH_3CHO (9.73×10^{-21} cm^2)[28] at 248 nm, ϕ_{CH_3I} and ϕ_{CH_3CHO} the CH_3 radical quantum yields for the 248 nm photolysis of CH_3I and CH_3CHO, respectively, and F_{248nm} the photolysis laser fluence. In Figure 2 are plotted for both species the absorption coefficient $\alpha_{t=0}$ as a function of the product of the CH_3I or CH_3CHO concentration multiplied by the corresponding absorption cross section at 248 nm: because all experiments have been carried out at the same photolysis energy (26 mJ cm^{-2}), F_{248nm} cancels out and this product is therefore a relative measure for the number of absorbed photons and with this the slope becomes a relative measure for the quantum yields ϕ_{CH_3I} and ϕ_{CH_3CHO}. Taking the ratio of both slopes ($m_{CH_3CHO} = (1.20 \pm 0.04) \times 10^{-3}$ and $m_{CH_3I} = (3.345 \pm 0.07) \times 10^{-3}$), the absorption cross section $\sigma_{CH_3O_2}$ cancels out as well and the ratio of the CH_3 radical quantum yields for both photolysis reactions is obtained.

A small correction needs to be applied to the CH_3O_2 absorption coefficient obtained following the photolysis of CH_3I: from an extrapolation of α to zero delay, $\alpha_{CH_3I,t=0}$ is underestimated by around 10% due to a fast reaction sequence between CH_3O_2 and I-atoms and the subsequent reaction of

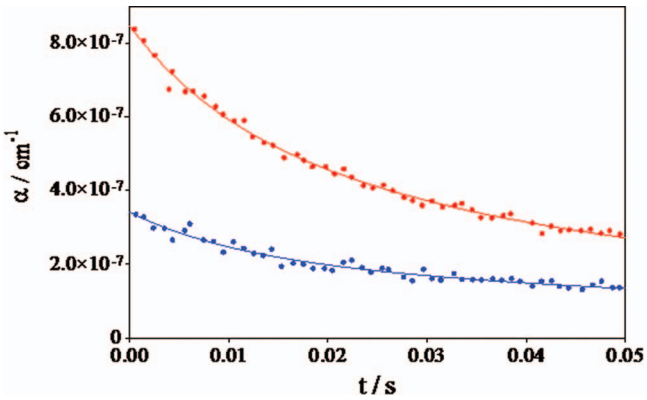

FIG. 1. CH_3O_2 profiles following the photolysis of 3.09×10^{14} cm^{-3} CH_3I (upper, red curve) and 2.87×10^{16} cm^{-3} CH_3CHO (lower, blue curve) in the presence of $[O_2] = 5.7 \times 10^{17}$ cm^{-3}. The maximum α corresponds to a concentration of $[CH_3O_2] \approx 2 \times 10^{13}$ cm^{-3}.

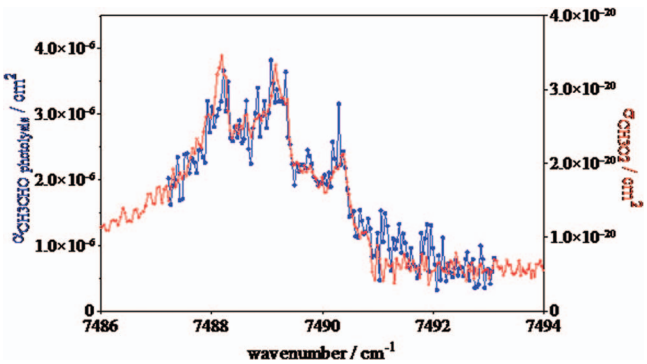

FIG. 3. Relative absorption spectrum obtained following the 248 nm photolysis of CH_3CHO (blue, left y-axis) compared to the absolute CH_3O_2 absorption spectrum obtained by Farago *et al.*[20] following the 248 nm photolysis of CH_3I (red, right y-axis).

CH_3O_2I with I-atoms.[29] This reaction sequence decreases the CH_3O_2 concentration by around 10% on the millisecond time scale (for more details see Bossolasco *et al.*[30]) and hence the slope for the CH_3I photolysis in Figure 2 is also underestimated by around 10%. Taking this into account and applying the recommended[31] CH_3 radical yield for the 248 nm photolysis of CH_3I of $\phi_{CH_3I} = 1$, one obtains a CH_3 radical yield for the 248 nm photolysis of CH_3CHO of $\phi = 0.33$.

An overestimation of the CH_3 radical yield could arise from the possible formation of other products in reaction (R1a)–(R1f) absorbing in the near infrared and thus faking a higher CH_3O_2 concentration. Unfortunately, the absorption spectrum of CH_3O_2 radicals in this wavelength range is rather broad[20] and hence it is not possible to shift the wavelength of the DFB laser off the absorption line to unravel any other, broadband absorbing by-products. Therefore, we have measured the absorption spectrum following the photolysis of CH_3CHO over a large wavelength range, covering a characteristic structure of the ν_{12} transition of the CH_3O_2 absorption spectrum including three distinct absorption peaks. Even though the S/N ratio is rather poor

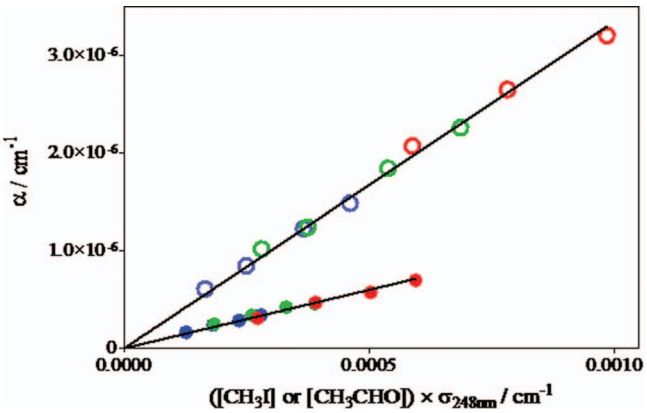

FIG. 2. Absorption coefficient α as a function of the product of precursor concentration multiplied by absorption coefficient, photolysis energy was kept constant for all experiments (26 mJ cm^{-2}): open symbols CH_3I, filled symbols CH_3CHO. Blue circles: p = 50 Torr, $[O_2] = 5.7 \times 10^{17}$ cm^{-3}; green circles: p = 50 Torr, $[O_2] = 8.2 \times 10^{17}$ cm^{-3}; red circles: p = 100 Torr, $[O_2] = 3.3 \times 10^{18}$ cm^{-3}.

following the CH_3CHO photolysis (blue line) due to the small absorption cross section of CH_3CHO, a very good agreement is found with the shape of the CH_3O_2 spectrum (Figure 3), obtained from the photolysis of CH_3I.[20] From this experiment we conclude that a contribution of other, unknown absorbing species to the absorption signal is unlikely.

The error in the determination of the CH_3 quantum yield lies mostly in the uncertainty of the absorption cross sections of the two precursors, CH_3I and CH_3CHO. We have used for both species the values recommended by the IUPAC committee,[28] only slightly different from JPL recommendation.[32] For CH_3I, the IUPAC value (8.07×10^{-19} cm^2) is based on the measurements of Roehl *et al.*,[33] Jenkin *et al.*[34] and Rattigan *et al.*,[35] while the JPL recommendation[32] include also the value obtained by Fahr *et al.*,[36] leading to a 4% higher value (8.40×10^{-19} cm^2). For CH_3CHO, the IUPAC recommendation (9.73×10^{-21} cm^2) reflects the data of Martinez *et al.*,[37] while JPL recommends a 6% higher value (10.33×10^{-21} cm^2) by including data published in the PhD thesis of H. G. Libuda (University Wuppertal, 1992). Another small error is caused by the correction necessary for the CH_3O_2 concentration from CH_3I photolysis due to secondary chemistry. However, this correction itself is only small (10%), and hence a minor error would only have a small impact on the CH_3 radical yield of the CH_3CHO photolysis. Other errors such as concentration, pressure, photolysis energy, absorption path length are all cancelled out due to the relative measurement. We therefore estimate the uncertainty on the CH_3 radical yield to be less than 10%:

$$\phi_{CH_3} = 0.33 \pm 0.03.$$

This unequivocal, non-negligible yield of CH_3 radials is in contradiction with the results of Rubio-Lago *et al.*,[9,10] who did not observe any CH_3 signal in their experiments, using two different detection techniques for CH_3 radicals, but this might be explained according to the authors by a low sensitivity of their technique for CH_3 radicals. The result is, however, in satisfactory agreement with the theoretical work of Han *et al.*[13] predicting an overall CH_3 yield of 60% following 230 nm photolysis.

B. Pressure broadening of HO_2 absorption line

The HO_2 absorption spectrum in the near infrared has been recorded by Thiébaud *et al.*[19] in the wavelength range between 6600 cm^{-1} and 6700 cm^{-1}. They observed the strongest line at 6638.205 cm^{-1}, with an absorption cross section twice as high as all other lines in that spectral range. It is therefore likely that the line consists of the superposition of two individual lines. Even though this line has been employed for the quantification of HO_2 in many studies,[38,39] the pressure broadening behaviour of this particular line has rarely been investigated. Thiebaud *et al.*[19] have determined the helium pressure broadening of a line at 6637.29 cm^{-1} using two different methods: (a) scanning the full line at different pressures and fit the shape to a Voigt profile and (b) measuring the absolute peak absorption cross section from kinetic decays and extract the pressure broadening coefficient by supposing a Voigt profile and imposing the Doppler linewidth at zero pressure. Both methods led to a good agreement for this line with a broadening coefficient of $\gamma_{He} = 0.057$ cm^{-1} atm^{-1}. In that work, only the peak absorption cross section in 50 Torr He was determined from kinetic measurements for the strongest line at 6638.205 cm^{-1}. Ibrahim *et al.*[40] have measured the air broadening coefficients for 34 HO_2 absorption lines in this wavelength range, yielding quantum number dependant broadening coefficients between 0.09 and 0.14 cm^{-1} atm^{-1}; the line at 6638.205 cm^{-1}, however, has not been studied in that work. In a recent paper, Tang *et al.*[41] have studied the broadening behaviour of the strongest HO_2 line by measuring the peak absorption coefficient at different pressures and retrieved air broadening coefficients supposing a Voigt profile and Doppler width at zero pressure. After applying a correction due to instrumental broadening, a broadening coefficient of $\gamma_{air} = 0.106$ cm^{-1} atm^{-1} was obtained. By comparison with the peak absorption in helium they estimate $\gamma_{He} = 0.035$ cm^{-1} atm^{-1}.

However, the strong line being probably the superposition of two individual lines, it cannot be excluded, that the superposition is not perfect and that the two lines are slightly shifted. This would result in a line width at zero pressure larger than the theoretical Doppler width, and hence it could be hazardous to deduce pressure dependant peak absorption cross sections by supposing the theoretical Doppler width at zero pressure. Because the determination of the HO_2 quantum yield at different pressures requires accurate knowledge of the pressure dependant absorption cross section, we have determined the helium pressure broadening of the absorption line at 6638.205 cm^{-1}. The full as well as an adjacent smaller line, centred at 6638.12 cm^{-1}, have been scanned at four different pressures between 10 and 95 Torr helium and both lines have been fitted to a Voigt profile using the Fityk Software.[42] In these experiments, HO_2 radicals have been generated by 248 nm photolysis of $COCl_2$ in the presence of excess CH_3OH and O_2, a clean source for the preparation of HO_2 radicals. The absorption lines have been scanned by measuring successively kinetic decays under identical experimental conditions (precursor and bath gas concentration as well as photolysis energy) at different wavelengths. The wavelength has been automatically incremented by around 0.001 cm^{-1} through a LabView program as soon as enough ring-down events (user-defined as 20 ring-down events in the first 5 ms following the photolysis pulse) had occurred to describe the HO_2 decay; this condition was generally fulfilled after less than five photolysis pulses. The time resolved ring-down events have been converted to absorption coefficients α using Eq. (1). Each kinetic trace has then been fitted in order to retrieve by extrapolation the absorption coefficient $\alpha_{t=0}$, i.e., the absorption coefficient at zero delay after the photolysis laser (more details on this method can be found in Jain *et al.*[24]). The result is presented in Figure 4 for all pressures with each data point being the result of one kinetic decay. The full line represents a fit to a Voigt profile, the absorption coefficients α have been normalized to the surface area such as obtained from the Voigt fitting for each pressure. It can be seen in Figure 4, that the peak absorption coefficient decreases only by around 15% with the pressure increasing from 10 to 95 Torr He, pointing to a weak pressure broadening.

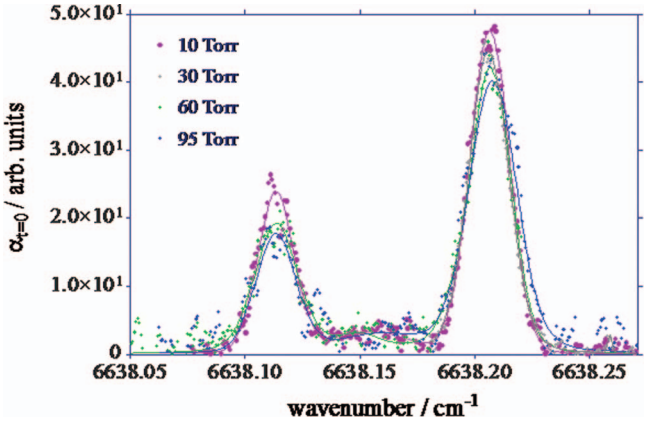

FIG. 4. HO_2 absorption lines at 10, 30, 60, and 95 Torr helium. The spectra have been scaled to the line strength of the line at 6638.205 cm^{-1}, such as obtained from the Voigt fit.

In Figure 5 are plotted the line widths (half width at half maximum, HWHM), such as obtained from the fitting procedure, as a function of pressure for both lines: a very weak broadening coefficient is obtained for both lines with an

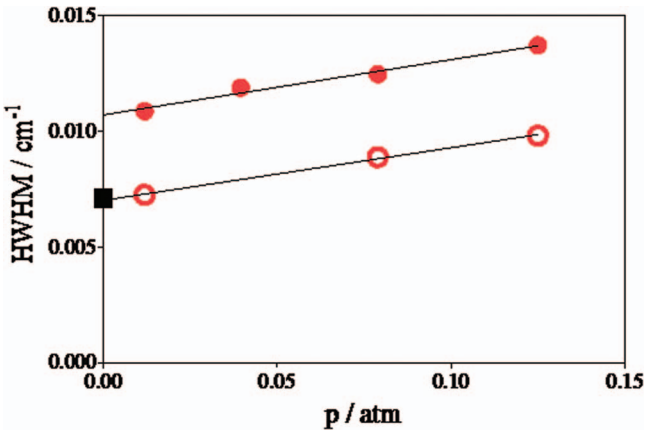

FIG. 5. Linewidth (HWHM) of both lines from Figure 4 at the four different pressures (no data available for the small line at 30 Torr): filled red circles 6638.205 cm^{-1}, open red circles 6638.12 cm^{-1}, and black square: theoretical Doppler line width.

average value of $\gamma_{He} = 0.0237$ cm^{-1} atm^{-1}. It can also be seen in Figure 5 that the line width extrapolated to zero pressure (10.72×10^{-3} cm^{-1} HWHM) is not in agreement with the theoretical Doppler width (7.088×10^{-3} cm^{-1} HWHM; represented as a black dot in Figure 5) for the strong line at 6638.205 cm^{-1}, while the extrapolation is in excellent agreement with the expected value for the smaller line at 6638.12 cm^{-1}. Nonetheless, this result is consistent with the suspicion of the line at 6638.205 cm^{-1} being composed of two individual, slightly shifted absorption lines. Using these values, a line strength of $S = 7.09 \times 10^{-21}$ cm^{-1} can be deduced by adjusting the peak absorption cross section at 50 Torr helium, obtained by Thiébaud *et al.*[19] (2.72×10^{-19} cm^2), to a Voigt profile.

Based on these measurements, the following pressure dependant absorption cross sections have been used in what follows to convert ring-down times into absolute HO_2 concentrations: $\sigma_{6638.205\ cm\text{-}1} = 3.02$, 2.72 and 2.49×10^{-19} cm^2 at 10, 50, and 90 Torr, respectively.

C. HCO radicals and H-atom quantum yield from time resolved HO_2 profiles

Continuous wave cavity ring-down spectroscopy (cw-CRDS) was used to monitor the time resolved profiles of HO_2 radicals formed after the 248 nm photolysis of CH_3CHO at pressures between 10 and 90 Torr He. Both primary photolysis products, HCO radicals from reaction (R1a) and H atoms from reaction (R1e) and possibly (R1c), can be converted into HO_2 radicals via reaction with O_2:

$$HCO + O_2 \rightarrow CO + HO_2, \qquad (R3)$$

$$H + O_2(+M) \rightarrow HO_2(+M). \qquad (R4)$$

The rate constants of both reactions differ by around two to three orders of magnitude, which allow distinguishing HCO radicals from H atoms by using different O_2 concentrations. The principle of this technique has been shown recently in a work on the photolysis of CF_3CH_2CHO:[43] reaction (R3) is independent of total pressure[28] with $k_3 = 5.2 \times 10^{-12}$ cm^3 s^{-1}, while the rate constant for reaction (R4) depends on pressure and bath gas: for He, the low pressure limit[44] is $k_{4,0} = 1.8 \times 10^{-32}$ cm^6 molecule^{-2} s^{-1}, i.e., $k_4 = 0.59$, 2.97 and 5.35×10^{-14} cm^3 s^{-1} at 10, 50, and 90 Torr He, respectively. At the lowest O_2 concentrations used in this work (few 10^{15} molecule cm^{-3}), HCO is converted into HO_2 within less than one millisecond, while at the highest O_2 concentrations (above 10^{17} molecule cm^{-3}) both, HCO radicals and most of the H atoms are convert into HO_2 on a much shorter time scale.

Figure 6 shows a typical example for a series of experiments with increasing O_2 concentration. At the lowest O_2 concentration (0.16×10^{16} cm^{-3} in the example of Figure 6, red dots) only HCO is converted to HO_2, while H atoms will react with acetaldehyde:

$$H + CH_3CHO \rightarrow H_2 + CH_3CO. \qquad (R5)$$

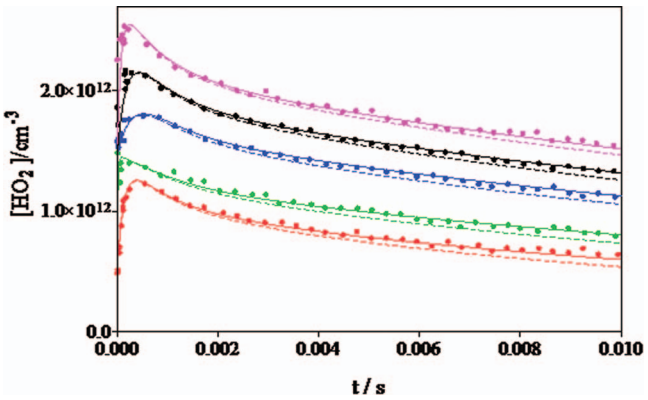

FIG. 6. HO_2 concentration time profiles at five different of O_2 at a total pressure of 50 Torr helium. $[CH_3CHO] = 1.67 \times 10^{16}$ cm^{-3}, photolysis laser fluence of 37.1 mJ cm^{-2}. O_2 concentrations were 0.16, 1.23, 5.60, 12, and 31×10^{16} cm^{-3}, from bottom to top. Data points at the first 200 μs are from individual ring down events, thereafter ring down events have been averaged within 300 μs time windows. Full lines from model Table I, dashed lines same model except rate constants for R20a and b from Groß *et al.*[45]

The rate constant k_5 (1.1×10^{-13} cm^3 molecule^{-1} s^{-1})[46] is between 2 and 20 times faster than k_4 in our pressure range and leads to a pseudo-first order decay of around 1000 s^{-1} for H atoms, compared to a pseudo-first order rate of less than 100 s^{-1} for reaction (R4) under low O_2-concentrations. With increasing O_2 concentration, the rate of reaction (R3) increases and is in the example of Figure 6 only barely resolved at the second lowest O_2-concentration ($[O_2] = 1.23 \times 10^{16}$ cm^{-3}, green dots). Under these conditions the conversion of HCO is completed within a few tens of μs and the HO_2 concentration decreases following this near-instantaneous rise, because the conversion of H-atoms into HO_2 is still too slow to compete with reaction (R5). With further increase in the O_2 concentration (5.60×10^{16} cm^{-3}, blue dots), another increase of HO_2 is to be seen over the first ms, due to an increased competition of reaction (R4) compared to reaction (R5). At even higher O_2 concentrations (3.1×10^{17} cm^{-3}), the HO_2 concentration further increases as now H-atoms are more and more converted to HO_2 instead of reacting through (R5): the pseudo-first order rate constant for reaction (R4) under these conditions is 9000 s^{-1}, one order of magnitude faster than reaction (R5).

In order to retrieve the H atom and HCO radical yields, profiles such as shown in Figure 6 have been fitted to a chemical mechanism including the mentioned reactions as well as other reactions known to influence the HO_2 concentrations-time profile on a short time scale (see Table I). However, first attempts of reproducing HO_2 profiles obtained at the lowest O_2 concentrations pointed to the existence of an HO_2 formation path other than reaction (R3) or (R4): a very rapid formation of HO_2 radicals is observed, much faster than expected from the well-known rate constant of reaction (R3) and not resolved with the time resolution of our experiment, even at the lowest O_2 concentrations.

Figure 7 shows a zoom of the first ms of examples obtained at 90 Torr total pressure under low O_2 concentrations: initial CH_3CHO and O_2 concentrations are the same for all experiments, only the photolysis energy has been varied. Under these O_2 concentrations, reaction (R3) has a pseudo-first

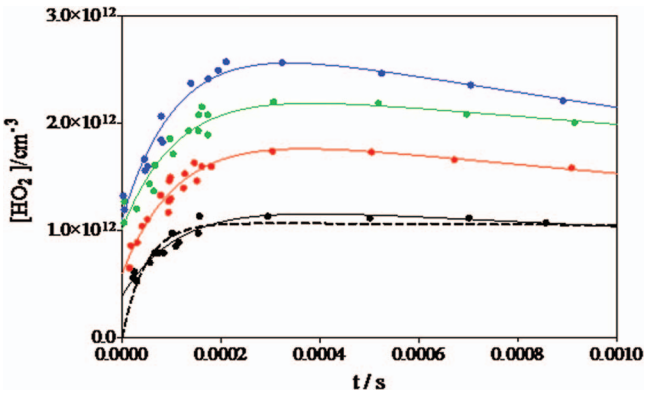

FIG. 7. HO_2 concentration time profiles at 90 Torr helium. $[CH_3CHO] = 1.67 \times 10^{16}$ cm^{-3}, $[O_2] = 1.6 \times 10^{15}$ cm^{-3}, photolysis energy was 26.4, 47.8, 63.8, and 81.1 mJ cm^{-2} from bottom to top. Full lines represent a fit to (2), fixing only k_{fast} to the expected pseudo first order rate for reaction (R3), dashed line represents fit forced through origin. Data points at the first 200 μs are individual ring down events, thereafter ring down events have been averaged within 200 μs time windows.

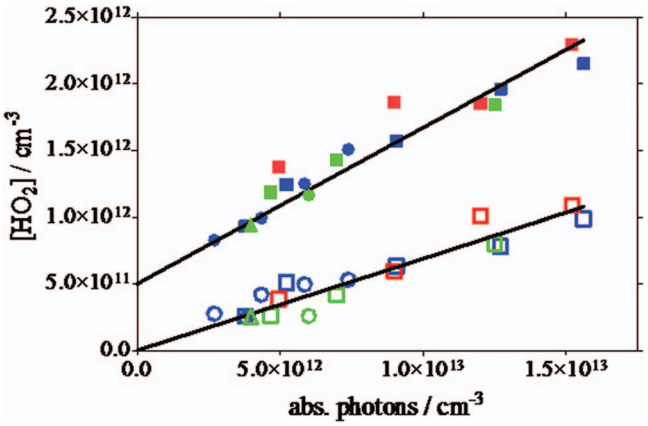

FIG. 8. Plot of $[HO_2]_{ini}$ (open symbols) and $[HO_2]_{sec}$ (filled symbols, shifted by 5×10^{11} cm^{-3} for better visibility) as a function of absorbed photons such as obtained from Figure 7-type fits: total pressure is 90 (red symbols), 50 (green symbols), and 10 Torr (blue symbols). $[CH_3CHO] = 16.7$ (squares), 8.1 (circles), and 5.3 (triangle) $\times 10^{15}$ cm^{-3}, photolysis energy has been varied between 24 and 82 mJ cm^{-2}.

order rate of 8400 s^{-1} and is with a rise time of around 200 μs well resolved in our experiments. HO_2 concentration time profiles have been fitted to an association reaction (k_{fast}), followed by a much slower decay (k_{slow})

$$[HO_2] = [HO_2]_{ini} \times e^{-k_{slow}t} + [HO_2]_{sec} \times \frac{k_{fast}}{k_{slow} - k_{fast}}(e^{-k_{fast}t} - e^{-k_{slow}t}), \quad (2)$$

whereby k_{fast} can be associated to the pseudo-first order rate of reaction (R3), k_3', while k_{slow} corresponds to loss of HO_2 radicals by diffusion and other secondary reactions. Such fits returned a time constant for k_{fast} in good agreement with k_3' only when a non-zero value for $[HO_2]_{ini}$ was admitted, i.e., the formation of HO_2 immediately (on our time scale) after the photolysis pulse. Forcing $[HO_2]_{ini}$ to zero returned poor quality fits with values for k_3' more than a factor of two faster than would be expected from the measured O_2 concentration: such a fit is shown in Figure 7 as a dashed line for the lowest photolysis energy ($k_{fast} = 21\,500$ s^{-1} instead of 8400 s^{-1} as fixed for all full line). Therefore, we suspect that another pathway of HO_2 radical formation exists following the 248 nm excitation of CH_3CHO in the presence of O_2, not mentioned in the literature to our knowledge. The reaction seems to be completed within the first 10 μs, leading with an O_2 concentration on the order of 10^{15} cm^{-3} to a rate constant for this reaction near collision frequency.

Rapid initial HO_2 formation has already been observed in our group following the 248 nm excitation of C_6H_6 in the presence of O_2 whereby it turned out that 2-photon absorption by C_6H_6 was at the origin of the very fast HO_2 formation.[47] In order to test for a possible 2-photon process as the origin of the rapid HO_2 formation, we have carried out experiments with varying photolysis energy (24–82 mJ cm^{-2}). Three sets of experiments such as shown in Figure 7 were carried out at 10 Torr with $[CH_3CHO] = 1.67$ and 0.80×10^{16} cm^{-3} and at 90 Torr with $[CH_3CHO] = 1.63 \times 10^{16}$ cm^{-3} as well as 5 experiments at 50 Torr.

Figure 8 summarizes the concentrations of $[HO_2]_{ini}$ and $[HO_2]_{sec}$ such as returned by the fit to (2) for all experiments with low O_2 concentrations as a function of absorbed photons. In all fits, the rate constant k_{fast} was forced to the expected pseudo-first order rate constant k_3'. No systematic dependence of the yields on the total pressure (different colours), the laser energy (same symbol, but different number of absorbed photons), or the CH_3CHO concentration (different symbols) was observed. The yields such as obtained from the slope of the regression through all data leads to a yield of $\phi_{ini} = 0.069 \pm 0.003$ and $\phi_{sec} = 0.117 \pm 0.009$ (errors are statistical only).

The origin of the rapid HO_2 is unknown: to our knowledge no such pathway has been mentioned in the literature. One option would be a reaction between highly excited HCO radicals and O_2, possibly faster than reaction (R3). In this case, one could expect that more HCO would be stabilized at 90 Torr He compared to 10 Torr He, thus increasing the branching of $[HO_2]_{sec}$ compared to $[HO_2]_{ini}$ with increasing pressure. However, we do not see any pressure dependence of the ratio $[HO_2]_{ini}$ to $[HO_2]_{sec}$ within the experimental uncertainty, the yields of both HO_2 are pressure independent (see symbols with different colours in Figure 8). Another argument against the excited HCO-hypothesis is that from arithmetic considerations the CH_3 radical does not seem to be the co-product of this reaction (see next paragraph). Chubb *et al.*[48] have recently described the formation of vinyl alcohol as the result of phototautomerization of acetaldehyde following its excitation in the wavelength range 295–335 nm at low pressure: quantum yields of up to 7.7% were determined at 330 nm and 20 Torr. It can be speculated that the initially formed, excited vinyl alcohol might further react with O_2 to lead to vinoxy radicals and HO_2. However, in the frame of this work no conclusion can be drawn about the origin of the prompt HO_2 and we therefore tentatively propose a rapid reaction between excited CH_3CHO^* and O_2:

$$CH_3CHO^* \xrightarrow{O_2} HO_2 + CH_3CO, \quad (R1f)$$

with formation of the acetyl radical, CH_3CO, as the co-product. Further research is needed to elucidate the formation pathway of the prompt HO_2.

The final yields of radical formation through the three channels (R1a), (R1e), and (R1f) following the 248 nm photolysis of CH_3CHO were retrieved from fitting $[HO_2]$ profiles to the complete model such as given in Table I, thus taking into account secondary reactions. Six sets of experiments, such as shown in Figure 6, were carried out under the following conditions: 50 Torr : $[CH_3CHO]/10^{16}$ cm^{-3}: F/mJ cm^{-2} = 1.67:24.8, 1.67:37.1, 1.67:66.4, 0.81: 66.4; 0.53:66.6 and 10 Torr: 0.53/67.0. The model reproduces perfectly well such as shown in Figure 6, within better than ±12%, all HO_2 profiles under all conditions with the following yields: $\phi_{1a} = 0.125$, $\phi_{1e} = 0.205$ and $\phi_{1f} = 0.07$.

The yield of reaction (R1a) is slightly higher than the slope of the "slow" HO_2 of Figure 8 (0.117): all experiments in Figure 8 where carried out under very low O_2 concentrations, and thus the very fast radical-radical reactions, such as $CH_3 + HCO$ ($k_6 = 2 \times 10^{-10}$ cm^3 $molecule^{-1}$ s^{-1})[49] or $H + HCO$ ($k_7 = 1.5 \times 10^{-10}$ cm^3 $molecule^{-1}$ s^{-1}),[50] have a slight impact on the observed maximal HO_2 radical concentration under these conditions, leading to a lower apparent yield in Figure 8. These reactions are taken into account when fitting to the full model (reactions 6 to 11) and hence the HCO radical yield is slightly higher.

The dashed lines in Figure 6 shows a fit using the same chemical model as for the full lines, only the rate constant for the reaction of $CH_3C(O)O_2$ with HO_2 radicals (reaction 20) was increased from 1.37 to 2.1×10^{-11} cm^3 s^{-1} (with, in addition, the yield of the radical pathway (a) increased from 0.45 to 0.61), corresponding to the most recent results from Groß *et al.*[45] It can be seen, that the peak HO_2 concentrations are not at all influenced by this change, only the HO_2 decay on longer time scales becomes faster. The model using the currently recommended rate constant for reaction (20) with the lower radical yield seems to better reproduce the experimental results. However, secondary chemistry influencing the HO_2 decay in this system on longer time scales (above 1 ms) is very complex, and the model used to fit the experiments such as shown in Table I is possibly not complete. Therefore, the current system is not sensitive enough to the rate constant of reaction (20).

The uncertainty on the HCO radical or the H atom yields, induced by uncertainties in the chemical model, is rather small. Experiments for a given condition (CH_3CHO concentration, laser energy and pressure) have always been carried out as a series with different O_2 concentrations and these series of experiments have then been fitted simultaneously to the same model, using a homemade, LabView based program. Doing so, uncertainties in the fate of the HCO radical under the lowest O_2 concentrations (red dots in Figure 6), when the lifetimes of H atoms, HCO and CH_3 radicals are long and poorly studied reactions such as $HCO + H$ or $HCO + CH_3$ have some importance, are eradicated at the next-higher O_2 concentration (green dots in Figure 6): now, the HCO-conversion to HO_2 is much faster than all secondary chemistry and the "starting" concentration of the green curve is governed by the total HCO yield. The fate of H-atoms is changing with increasing O_2 concentration and is, except for the lowest O_2 concentrations, when other radical-radical reactions such as (R2) and (R3) have some importance, divided between reactions (R4) and (R5). The increase of the termolecular rate constant of reaction (R4) due to the increased collision efficiency with increasing O_2 has been taken into account, based on the fall-off expressions from Fernandes *et al.*,[44] the most recent values have been taken for the rate constant of reaction (R5).[46] From the coherent, simultaneous fitting of the HO_2 profiles at the higher O_2 concentrations (above 5×10^{16} cm^{-3}) we conclude that the ratio of the rate constants k_4 and k_5 is well expressed. Also, the conversion of H atoms to HO_2 is around 90% at the highest O_2 concentration so that a small error in the ratio would have only a very minor impact on the retrieved H atom yield at this O_2 concentration.

From these considerations we conclude, that the major uncertainty in the H atom and HCO radical yield do not originate from possible uncertainties in the chemical model, but stem from the uncertainty in the determination of the photolysis energy and the absolute HO_2 concentration. The latter one is based on both, the HO_2 absorption cross section σ as well as the absorption path length R_L used in (1). Both values in turn are directly linked to the photolysis energy, as explained in the experimental section: the ratio R_L/σ, such as used in (1), has been found from separate H_2O_2 photolysis experiments to be coherent within better than 10% with the power meter reading. The same values (power meter reading, R_L and σ) are used for the CH_3CHO photolysis experiments, hence any systematic error in one of these values would cancel out. The error on the HCO radical and H atom quantum yields, combined from HO_2 quantification and fitting procedure, is therefore estimated to be ±20%.

$$CH_3CHO^* \rightarrow CH_3 + HCO \quad \phi_{1a} = 0.125 \pm 0.03, \qquad \text{(R1a)}$$

$$CH_3CHO^* \rightarrow CH_3 + H + CO \quad \phi_{1b} = 0.205 \pm 0.04, \qquad \text{(R1e)}$$

$$CH_3CHO^* \xrightarrow{O_2} CH_3CO + HO_2 \quad \phi_{1c} = 0.07 \pm 0.01. \qquad \text{(R1f)}$$

The agreement between the quantum yield for CH_3 radicals ($\phi_{CH_3} = 0.33 \pm 0.03$) and the sum of the quantum yields of (R1a) and (R1e) is excellent. From this agreement it can be presumed, that the triple fragmentation (R1e) is the major radical path following the 248 nm photolysis of acetaldehyde. A high yield of the reaction path (R1c) such as proposed by Mortgaat *et al.*,[3] ($\phi_{1c} = 0.12$ at 255 nm, with yield increasing with decreasing wavelength) does not seem to be consistent with our experimental data. Also, it seems unlikely, that the co-product of HO_2 radicals in reaction (R1f) is the CH_3 radicals, even if this possibility is within the combined uncertainties.

IV. CONCLUSION

We have directly measured the H atom, HCO and CH_3 radical yields following the 248 nm photolysis of acetaldehyde, CH_3CHO. Photolysis has been carried out in the presence of various amounts of O_2, and H atoms and HCO

radicals have been quantified as HO_2 radicals by cw-CRDS in the near infrared following their reaction with O_2. Yields of $\phi_H = 0.205 \pm 0.04$ and $\phi_{HCO} = 0.125 \pm 0.03$ have been obtained. In order to well reproduce the time resolved HO_2 profiles, another pathway forming very rapidly HO_2 radicals needed to be included with a rate constant near collision frequency: the yield of this pathway was found to be $\phi_{HO_2} = 0.07 \pm 0.01$. CH_3 radicals have been detected as CH_3O_2 radicals following their reaction with O_2. A yield of $\phi_{CH_3} = 0.33 \pm 0.03$ has been obtained in back-to-back experiments relative to the CH_3 radicals yield in the 248 nm photolysis of CH_3I. The results suggest that triple fragmentation is the major radical forming pathway following the 248 nm photolysis of CH_3CHO.

ACKNOWLEDGMENTS

This project was supported by the French ANR agency under Contract No. ANR-11-LabEx-0005-01 CaPPA (Chemical and Physical Properties of the Atmosphere). The laboratory PC2A participates in the Institut de Recherche en ENvironnement Industriel (IRENI) which is financed by Région Nord Pas-de-Calais, the Ministère de l'Enseignement Supérieur et de la Recherche, the CNRS and European Regional Development Fund (ERDF). The authors thank F. Rohart from PhLAM laboratory for helpful discussions about the HO_2 pressure broadening and E. P. Farago for assistance in some data treatment. A.B. thanks the European Community for a scholarship within the frame of the EuroTango project.

[1]D. B. Millet, A. Guenther, D. A. Siegel, N. B. Nelson, H. B. Singh, J. A. de Gouw, C. Warneke, J. Williams, G. Eerdekens, V. Sinha, T. Karl, F. Flocke, E. Apel, D. D. Riemer, P. I. Palmer, and M. Barkley, Atmos. Chem. Phys. **10**, 3405 (2010).
[2]K. R. Read, L. Carpenter, S. R. Arnold, R. Beale, P. Nightingale, J. R. Hopkins, A. C. Lewis, J. D. Lee, L. Mendes, and S. J. Pickering, Environ. Sci. Technol. **46**, 11028 (2012).
[3]G. K. Moortgat, H. Meyrahn, and P. Warneck, ChemPhysChem **11**, 3896 (2010).
[4]P. Warneck and G. K. Moortgat, Atmos. Environ. **62**, 153 (2012).
[5]D. Townsend, S. A. Lahankar, S. K. Lee, S. D. Chambreau, A. G. Suits, X. Zhang, J. Rheinecker, L. B. Harding, and J. M. Bowman, Science **306**, 1158 (2004).
[6]P. L. Houston and S. H. Kable, Proc. Natl. Acad. Sci. U.S.A. **103**, 16079 (2006).
[7]B. R. Heazlewood, M. J. T. Jordan, S. H. Kable, T. M. Selby, D. L. Osborn, B. C. Shepler, B. J. Braams, and J. M. Bowman, Proc. Natl. Acad. Sci. U.S.A. **105**, 12719 (2008).
[8]B. R. Heazlewood, S. J. Rowling, A. T. Maccarone, M. J. T. Jordan, and S. H. Kable, J. Chem. Phys. **130**, 054310 (2009).
[9]L. Rubio-Lago, G. A. Amaral, A. Arregui, J. G. Izquierdo, F. Wang, D. Zaouris, T. N. Kitsopoulos, and L. Banares, Phys. Chem. Chem. Phys. **9**, 6123 (2007).
[10]L. Rubio-Lago, G. A. Amaral, A. Arregui, J. Gonzalez-Vazquez, and L. Banares, Phys. Chem. Chem. Phys. **14**, 6067 (2012).
[11]J. M. Bowman and B. C. Shepler, Ann. Rev. Phys. Chem. **62**, 531 (2011).
[12]G. de Wit, B. R. Heazlewood, M. S. Quinn, A. T. Maccarone, K. Nauta, S. A. Reid, M. J. T. Jordan, and S. H. Kable, Faraday Discuss. **157**, 227 (2012).
[13]Y.-C. Han, B. C. Shepler, and J. M. Bowman, J. Phys. Chem. Lett. **2**, 1715 (2011).
[14]K.-C. Hung, P.-Y. Tsai, H.-K. Li, and K.-C. Lin, J. Chem. Phys. **140**, 064313 (2014).
[15]J. Thiebaud and C. Fittschen, Appl. Phys. B: Lasers Opt. **85**, 383 (2006).
[16]A. Parker, C. Jain, C. Schoemaecker, P. Szriftgiser, O. Votava, and C. Fittschen, Appl. Phys. B: Lasers Opt. **103**, 725 (2011).
[17]O. Votava, M. Masat, A. E. Parker, C. Jain, and C. Fittschen, Rev. Sci. Instrum. **83**, 043110 (2012).
[18]A. Parker, C. Jain, C. Schoemaecker, and C. Fittschen, React. Kinet. Catal. Lett. **96**, 291 (2009).
[19]J. Thiebaud, S. Crunaire, and C. Fittschen, J. Phys. Chem. A **111**, 6959 (2007).
[20]E. P. Faragó, B. Viskolcz, C. Schoemaecker, and C. Fittschen, J. Phys. Chem. A **117**, 12802 (2013).
[21]G. L. Vaghjiani and A. R. Ravishankara, J. Chem. Phys. **92**, 996 (1990).
[22]J. Thiebaud, A. Aluculesei, and C. Fittschen, J. Chem. Phys. **126**, 186101 (2007).
[23]R. Atkinson, D. L. Baulch, R. A. Cox, J. N. Crowley, R. F. Hampson, R. G. Hynes, M. E. Jenkin, M. J. Rossi, and J. Troe, Atmos. Chem. Phys. **4**, 1461 (2004).
[24]C. Jain, P. Morajkar, C. Schoemaecker, B. Viskolcz, and C. Fittschen, J. Phys. Chem. A **115**, 10720 (2011).
[25]P. Morajkar, C. Schoemaecker, and C. Fittschen, J. Mol. Spectrosc. **281**, 18 (2012).
[26]D. B. Atkinson and J. L. Spillman, J. Phys. Chem. A **106**, 8891 (2002).
[27]M. B. Pushkarsky, S. J. Zalyubovsky, and T. A. Miller, J. Chem. Phys. **112**., 10695 (2000).
[28]R. Atkinson, D. L. Baulch, R. A. Cox, J. N. Crowley, R. F. Hampson, R. G. Hynes, M. E. Jenkin, M. J. Rossi, and J. Troe, Atmos. Chem. Phys. **6**, 3625 (2006).
[29]T. J. Dillon, M. E. Tucceri, and J. N. Crowley, Phys. Chem. Chem. Phys. **8**, 5185 (2006).
[30]A. Bossolasco, E. P. Faragó, C. Schoemaecker, and C. Fittschen, Chem. Phys. Lett. **593**, 7 (2014).
[31]R. Atkinson, D. L. Baulch, R. A. Cox, J. N. Crowley, R. F. Hampson, R. G. Hynes, M. E. Jenkin, M. J. Rossi, J. Troe, and T. J. Wallington, Atmos. Chem. Phys. **8**, 4141 (2008).
[32]S. P. Sander, J. Abbatt, J. R. Barker, J. B. Burkholder, R. R. Friedl, D. M. Golden, R. E. Huie, C. E. Kolb, M. J. Kurylo, G. K. Moortgat, V. L. Orkin, and P. H. Wine, "Chemical Kinetics and Photochemical Data for Use in Atmospheric Studies, Evaluation No. 17," JPL Publication 10-6, Jet Propulsion Laboratory, Pasadena 2011.
[33]C. M. Roehl, J. B. Burkholder, G. K. Moortgat, A. R. Ravishankara, and P. J. Crutzen, J. Geophys. Res.: Atmos. **102**, 12819, doi:10.1029/97JD00530 (1997).
[34]M. E. Jenkin, T. P. Murrells, S. J. Shalliker, and G. D. Hayman, J. Chem. Soc., Faraday Trans. **89**, 433 (1993).
[35]O. V. Rattigan, D. E. Shallcross, and R. A. Cox, J. Chem. Soc., Faraday Trans. **93**, 2839 (1997).
[36]A. Fahr, A. K. Nayak, and M. J. Kurylo, Chem. Phys. **197**, 195 (1995).
[37]R. D. Martinez, A. A. Buitrago, N. W. Howell, C. H. Hearn, and J. A. Joens, Atmos. Environ. A **26**, 785 (1992).
[38]C. Jain, A. E. Parker, C. Schoemaecker, and C. Fittschen, ChemPhysChem **11**, 3867 (2010).
[39]M. Djehiche, A. Tomas, C. Fittschen, and P. Coddeville, Z. Phys. Chem. **225**, 938 (2011).
[40]N. Ibrahim, J. Thiebaud, J. Orphal, and C. Fittschen, J. Mol. Spectrosc. **242**, 64 (2007).
[41]Y. Tang, G. S. Tyndall, and J. J. Orlando, J. Phys. Chem. A **114**, 369 (2010).
[42]M. Wojdyr, J. Appl. Crystallogr. **43**, 1126 (2010).
[43]M. Antiñolo, C. Bettinelli, C. Jain, P. Dréan, B. Lemoine, J. Albaladejo, E. Jiménez, and C. Fittschen, J. Phys. Chem. A **117**, 10661 (2013).
[44]R. X. Fernandes, K. Luther, J. Troe, and V. G. Ushakov, Phys. Chem. Chem. Phys. **10**, 4313 (2008).
[45]C. B. M. Groß, T. J. Dillon, G. Schuster, J. Lelieveld, and J. N. Crowley, J. Phys. Chem. A **118**, 974 (2014).
[46]K. Ohmori, A. Miyoshi, H. Matsui, and N. Washida, J. Phys. Chem. **94**, 3253 (1990).
[47]C. Jain, P. Morajkar, C. Schoemaecker, and C. Fittschen, J. Phys. Chem. A **116**, 6231 (2012).
[48]A. E. Clubb, M. J. T. Jordan, S. H. Kable, and D. L. Osborn, J. Phys. Chem. Lett. **3**, 3522 (2012).
[49]W. Tsang and R. F. Hampson, J. Phys. Chem. Ref. Data **15**, 1087 (1986).
[50]D. L. Baulch, C. J. Cobos, R. A. Cox, C. Esser, P. Frank, T. Just, J. A. Kerr, M. J. Pilling, J. Troe, R. W. Walker, and J. Warnatz, J. Phys. Chem. Ref. Data **21**, 411 (1992).
[51]R. X. Fernandes, K. Luther, and J. Troe, J. Phys. Chem. A **110**, 4442 (2006).
[52]E. A. Selzer and K. D. Bayes, J. Phys. Chem. **87**, 392 (1983).

[53]D. L. Baulch, C. J. Cobos, R. A. Cox, P. Frank, G. Hayman, T. Just, J. A. Kerr, T. Murrells, M. J. Pilling, J. Troe, R. W. Walker, and J. Warnatz, J. Phys. Chem. Ref. Data **23**, 847 (1994).
[54]M. Sangwan and L. N. Krasnoperov, J. Phys. Chem. A **117**, 2916 (2013).
[55]P. Morajkar, C. Schoemaecker, M. Okumura, and C. Fittschen, Int. J. Chem. Kinet. **46**, 245 (2014).
[56]S. A. Carr, D. R. Glowacki, C.-H. Liang, M. T. Baeza-Romero, M. A. Blitz, M. J. Pilling, and P. W. Seakins, J. Phys. Chem. A **115**, 1069 (2011).
[57]C. Fittschen, B. Delcroix, N. Gomez, and P. Devolder, J. Chim. Phys. **95**, 2129 (1998).
[58]T. J. Dillon and J. N. Crowley, Atmos. Chem. Phys. **8**, 4877 (2008).